Available online at www.sciencedirect.com
SCIENCE DIRECT®
Journal of Solid State Chemistry 178 (2005) 2015–2023
JOURNAL OF SOLID STATE CHEMISTRY
www.elsevier.com/locate/jssc

Synthesis, crystal structures and ionic conductivities of $Bi_{14}P_4O_{31}$ and $Bi_{50}V_4O_{85}$. Two members of the series $Bi_{18-4m}M_{4m}O_{27+4m}$ (M = P, V) related to the fluorite-type structure

F. Mauvy, J.C. Launay, J. Darriet*

Institut de Chimie de la Matière Condensée de Bordeaux (ICMCB), UPR9048 CNRS, Université de Bordeaux 1, 87 Avenue du Docteur A. Schweitzer, Pessac Cedex 33608, France

Received 10 February 2005; received in revised form 22 March 2005; accepted 31 March 2005

Abstract

The two hitherto unknown compounds $Bi_{14}P_4O_{31}$ and $Bi_{50}V_4O_{85}$ were prepared by the direct solid-state reaction of Bi_2O_3 and $(NH_4)H_2PO_4$ or V_2O_5, respectively. $Bi_{14}P_4O_{31}$ crystallizes in a C-centred monoclinic symmetry ($C2/c$ space group) with the unit-cell parameters: $a = 19.2745(2)$ Å, $b = 11.3698(1)$ Å, $c = 52.4082(2)$ Å and $\beta = 93.63(1)^\circ$ ($Z = 16$). The symmetry of $Bi_{50}V_4O_{85}$ is also monoclinic ($I2/m$ space group) with lattice parameters of $a = 11.8123(3)$ Å, $b = 11.7425(2)$ Å, $c = 16.5396(2)$ Å and $\beta = 90.14(1)^\circ$ ($Z = 2$). Both structures correspond to a fluorite-type superstructure where the Bi and P or V atoms are ordered in the framework. An idealized structural model is proposed where the structures result of the stacking of mixed atomic layers of composition $[Bi_{14}M_4O_{31}]$ and $[Bi_{18}O_{27}]$ respectively. This new family can be formulated $Bi_{18-4m}M_{4m}O_{27+4m}$ with M = P, V and where the parameter m ($0 \leqslant m \leqslant 1$) represents the ratio of the number of $[Bi_{14}M_4O_{31}]$ layers to the total number of layers in the sequence. $Bi_{14}P_4O_{31}$ corresponds to $m = 1$ when $Bi_{50}V_8O_{85}$ corresponds to $m = 1/3$. In this last case, the structural sequence is simply one $[Bi_{14}V_4O_{31}]$ layer to two $[Bi_{18}O_{27}]$ layers. As predicted by the proposed structural building principle, $Bi_{14}P_4O_{31}$ is not a good ionic conductor. The conductivity at 650 °C is 4 orders of magnitude lower from those found in $Bi_{46}M_8O_{89}$ (M = P, V) ($m = 2/3$) and $Bi_{50}V_4O_{85}$ ($m = 1/3$).

Keywords: Phosphorous; Vanadium; Bismuth; Oxides; Crystal Structures; Fluorite-type superstructure; Ionic conductivity

1. Introduction

Defect fluorite-related solid-solution have largely been studied in the systems of Bi_2O_3–M_2O_5 (M = P, V, Nb, Ta) [1–10]. Indeed, substitution of Bi using pentavalent ions stabilizes the δ-Bi_2O_3 structure at room temperature when the δ-Bi_2O_3 variety is stable only between 937 K and the melting point of Bi_2O_3 at 1097 K. δ-Bi_2O_3 has been reported to have an oxygen deficient fluorite structure [11,12] in which structural disorder in the O sublattice is responsible for the high oxide ion conductivity of this phase.

Recently, it has been shown that the structures of $Bi_{46}M_8O_{89}$ (M = P, V) belong to this family and correspond to a fluorite type superstructure with $3 \times 3 \times 3$ subcells [13]. The cations are perfectly ordered in the fluorite framework and the M atoms occupy isolated MO_4 tetrahedra (M = P, V). The structure can be viewed as the stacking of two types of atomic layers with the compositions $[Bi_{18}O_{27}]$ and $[Bi_{14}M_4O_{31}]$ (M = P, V), respectively [13]. The sequence corresponds to: 2 $[Bi_{14}M_4O_{31}]$ layers + 1 $[Bi_{18}O_{27}]$ layer for $Bi_{46}M_8O_{89}$. From this description, by changing the sequence of these layers one can predict a series of phases based on the same building principle and therefore on can explain the 'large domain of solid-solution' of defect fluorite observed in these systems

*Corresponding author. Fax: +33 5 40 00 27 61.
E-mail address: darriet@icmcb-bordeaux.cnrs.fr (J. Darriet).

0022-4596/$ - see front matter © 2005 Elsevier Inc. All rights reserved.
doi:10.1016/j.jssc.2005.03.048

[2–9]. This paper is devoted to the synthesis, crystal structure and ionic conductivity of $Bi_{14}P_4O_{31}$ and $Bi_{50}V_8O_{85}$ which are two new members of this series.

2. Experimental

Powder sample of $Bi_{14}P_4O_{31}$ was prepared by solid-state reaction of stoichiometric amounts of the starting reagents Bi_2O_3 and $(NH_4)H_2PO_4$. The mixture was ground in an agate mortar and heated at 300 °C during 8 h and then at 800 °C for 12 h in gold crucible under an oxygen atmosphere. After grinding, the product was re-heated at 850 °C for 48 h. Further reheating at 850 °C did not show any evolution in the X-ray powder pattern.

Single crystals of $Bi_{14}P_4O_{31}$ were prepared by melting the powder sample at 950 °C followed by slow cooling at 5 °C/h down to room temperature. The selection of high quality single crystals was based upon size and the sharpness of the diffraction spots.

Powder sample of $Bi_{50}V_4O_{85}$ has been prepared by solid-state reaction from stoichiometric amounts of Bi_2O_3 and V_2O_5. After grinding, the mixture was heated at 920 °C in a gold crucible under oxygen flow during 48 h. At the end of the heating time, the product is quenched from 920 °C to room temperature in order to stabilize the desired phase. Indeed, annealing of $Bi_{50}V_4O_{85}$ at lower temperature gave rise to a decomposition in two phases: one being of sillenite type [14,15] and the second one being also related to fluorite type but with a composition richer in vanadium.

X-ray powder diffraction data were collected at room temperature over the angular range $5° \leqslant 2\theta \leqslant 80°$ with a step size of $\Delta(2\theta) = 0.02°$ using a Philips X-pert diffractometer operating with Cu$K\alpha$ radiation. The X-ray diffraction data were refined by a Le Bail profile analysis [16] using the Jana2000 program package [17]. The background was estimated by a Legendre polynom and the peak shapes were described by a pseudo-Voigt function varying five profile coefficients [18].

Single crystal X-ray diffraction data were collected on CCD-detector diffractometer with sealed-tube Mo$K\alpha$ X-ray source. Experimental details are summarized in Table 1. Data reduction was performed using the specific programs of the diffractometer and program package Jana2000 [17] was used for the numerical absorption correction and structure refinements. The shape of the crystal was determined via the video camera of the diffractometer.

Samples for impedance measurements were prepared as circular pellets with thickness, around $L = 0.15$ cm and surface area, around $S = 0.7\,cm^2$, sintered at 900 °C for 2 h. Electrical contacts were made of gold electrodes deposited on both surfaces of the sample in order to obtain a symmetrical cell.

Complex impedance spectroscopy measurements were carried out using a Solartron 1260 Frequency Response Analyzer. The frequency range was 10^{-1}–10^6 Hz with a signal amplitude of 50 mV. All these electrochemical experiments were performed at equilibrium from 400 °C up to 800 °C, i.e., under zero DC current intensity and under air over one cycle of heating and cooling. Impedance diagrams were analyzed and fitted using the Z view software. Resistance, capacitance and self values of equivalent circuits were thus obtained by least square refinement.

Table 1
Crystallographic data for $Bi_{14}P_4O_{31}$

Physical, crystallographic and analytical data	
Formula	$Bi_{14}P_4O_{31}$
Crystal colour	Pale green
M_W (g mol^{-1})	3545.6
Crystal system	Monoclinic
Space group	$C2/c$
Parameters	$a = 19.2745(4)$ Å, $b = 11.3698(4)$ Å, $c = 52.4082(4)$ Å, $\beta = 93.63(3)°$
V (Å^3)	11462.1(5)
Z	16
Density calc. (g cm^{-3})	8.22
Crystal shape	Unshaped
Crystal size (mm)	$0.035 \times 0.018 \times 0.0025$
Data Collection	
Temperature	RT
Diffractometer	Bruker-Nonius KappaCCD
Radiation	Mo$K\alpha$ ($\lambda = 0.71069$ Å)
Scan mode	CCD scan
$h\,k\,l$ range	$-30<h<31$ $-17<k<18$ $-84<l<65$
θ_{max}	35°
Data reduction	
Linear absorption coeff.	91.83 mm^{-1}
Absorption correction	Gaussian
T_{min}/T_{max}	0.009/0.110
No of reflections	24961
No of independent reflections	9442
Criterion for obs. reflections	$I > 3\sigma(I)$
Refinement results	
Refinement	F^2
$F(000)$	23520
R factors	$R(F) = 0.0583$, $wR(F^2) = 0.1250$
No of refined parameters	574
g.o.f.	1.12
Weighting scheme	$w = 1/(\sigma^2(I) + 0.0009I^2)$
Diff. Fourier residues (e$^-$/Å^3)	[−3.67, +3.58]

3. Results and discussion

3.1. $Bi_{14}P_4O_{31}$

The initial unit cell was determined using a standard peak search of the selected single crystal. $Bi_{14}P_4O_{31}$ crystallizes in a *C*-centred monoclinic symmetry. The observed extinction rule suggests the space groups $C2/c$ or Cc. The final unit cell parameters: $a = 19.2745(2)$ Å, $b = 11.3698(1)$ Å, $c = 52.4082(2)$ Å and $\beta = 93.63(1)^\circ$ were obtained and refined using the X-ray powder pattern (Fig. 1). All the peaks are indexed even the weak peaks as shown in Fig. 1(b). The strongest reflections correspond to a fluorite subcell. The relationships between the monoclinic cell and the cubic fluorite subcell ($a_c \approx 5.5$ Å) are:

$$\mathbf{a} = \frac{3}{2}\mathbf{a_c} + \frac{3}{2}\mathbf{b_c} + 3\mathbf{c_c},$$

$$\mathbf{b} = -\frac{3}{2}\mathbf{a_c} + \frac{3}{2}\mathbf{b_c},$$

$$\mathbf{c} = -6\mathbf{a_c} - 6\mathbf{b_c} + 4\mathbf{c_c},$$

where $\mathbf{a_c}$, $\mathbf{b_c}$ and $\mathbf{c_c}$ are the unit-cell vectors of the prototypic cubic fluorite. Therefore the volume of the superstructure is 72 times larger than the elementary volume of the fluorite. The structure was solved in the centrosymmetric $C2/c$ space group. The positions of the heavy atoms were deduced by the Patterson method. The 288 heavy atoms of the unit cell are distributed in 8 general positions for P and 28 general positions for Bi. The oxygen atoms were deduced from successive difference Fourier maps. Clearly, 62 oxygen positions have been localized which are fully occupied. The formula corresponds to the expected chemical composition $Bi_{14}P_4O_{31}$ with $Z = 16$. The residual R factor converged to $R = 0.0583$ for 9442 observed reflections with only anisotropic displacements factors for the bismuth and the phosphorous atoms (Table 1). Final parameters are gathered in Table 2.

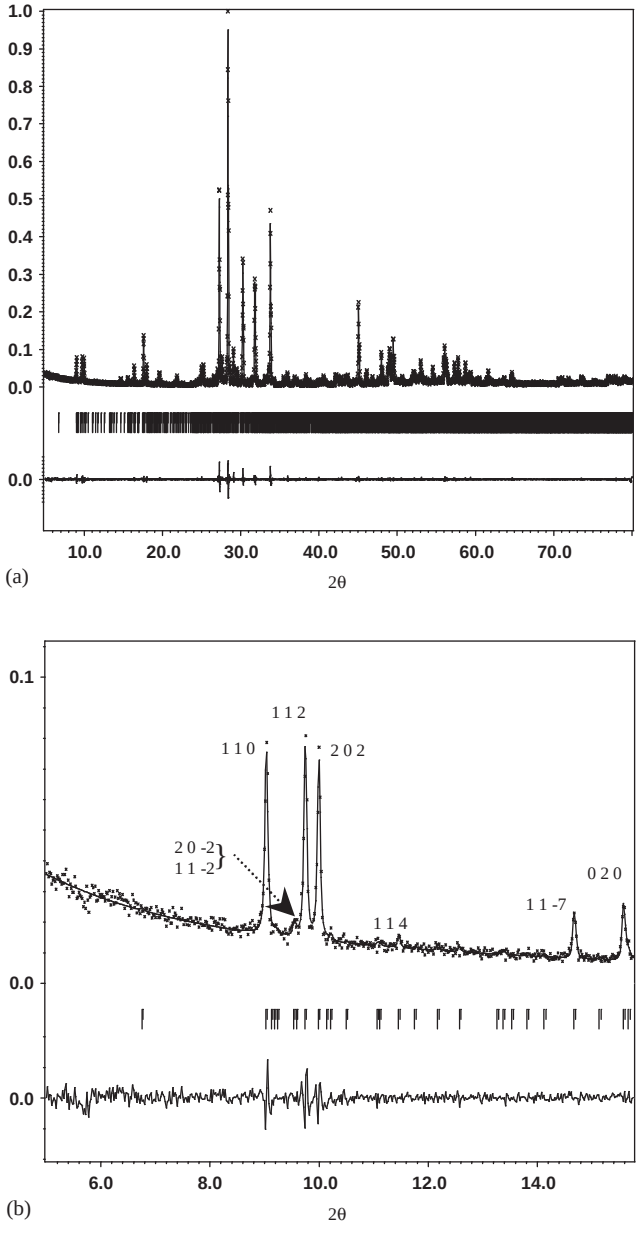

Fig. 1. (a) XRD powder pattern of $Bi_{14}P_4O_{31}$, and (b) zoom at low2θ-angles showing the indexation of the weak peaks.

The structure corresponds to a fluorite-type superstructure where the Bi and P atoms are perfectly ordered. A projection of the structure of $Bi_{14}P_4O_{31}$ on the (010) plane is given in Fig. 2. As observed in the structures of $Bi_{46}M_8O_{89}$ (M = P, V), the PO_4 tetrahedra are isolated from one another. The P–O distances are compiled in Table 3. The phosphorous–oxygen distances range between 1.46(2) and 1.61(2) Å and are consistent with the distances noted in the literature. Like in the structures of $Bi_{46}M_8O_{89}$ (M = P, V), the $6s^2$ lone pair of Bi^{III} is stereochemically active and the coordination numbers vary from CN = 3 to 5 (Fig. 3) if one limits the Bi–O distances involved in the surroundings to 2.5 Å. Further details of the Bi–O distances can be obtained from the supporting information available from the Fachinformationszntrum Karlsruhe, 76344 Eggenstein-Leopoldshafen, Germany, (fax: (49) 7247-808-666; email: mailto:crysdata@fiz-karlsruhe.de) on quoting the depository number CSD-415115.

The structure can be viewed as the stacking of $[Bi_{14}P_4O_{31}]$ layers parallel to the (xy0) plane of the monoclinic cell with a periodicity of 16 layers along the c-axis (Fig. 4). The main feature of the structure is that all the oxygen positions are fully occupied and therefore the structure is totally ordered (Table 2). This result differs from the structure of $Bi_{46}M_8O_{89}$ (M = P, V) where some oxygen positions are partially occupied [13]. As it will be shown latter, this result will be confirmed by ionic conductivity measurements. The structure of

Table 2
Final coordinates, equivalent displacement parameters (Bi, P) and isotropic displacement parameters (O) for $Bi_{14}P_4O_{31}$

Atoms	x	y	z	$U_{eq}(Å^2)/U_{iso}(Å^2)$
P1	0.1488(5)	0.3900(8)	0.1598(1)	0.015(2)
P2	0.4789(5)	0.3872(7)	0.1549(1)	0.013(2)
P3	0.0556(4)	0.1024(7)	0.0910(1)	0.009(2)
P4	0.2302(4)	0.5920(8)	0.0998(1)	0.011(2)
P5	0.2980(4)	0.3905(7)	0.0360(1)	0.011(2)
P6	0.1205(4)	0.8987(7)	0.0267(1)	0.008(2)
P7	0.0978(4)	0.6090(7)	0.2252(1)	0.012(2)
P8	0.4202(4)	0.6022(7)	0.2178(2)	0.014(2)
Bi1	0.309916)	0.5797(1)	0.15606(2)	0.0111(3)
Bi2	0.31428(6)	0.9055(1)	0.15198(2)	0.0118(3)
Bi3	0.31707(6)	0.2207(1)	0.15200(2)	0.0133(3)
Bi4	0.15235(6)	0.0725(1)	0.14784(2)	0.0119(3)
Bi5	0.14970(6)	0.7526(1)	0.16244(2)	0.0131(3)
Bi6	0.49188(6)	0.0460(1)	0.15593(2)	0.0128(3)
Bi7	0.47942(6)	0.7321(1)	0.15941(2)	0.0134(3)
Bi8	0.40087(6)	0.4435(1)	0.28029(2)	0.0124(3)
Bi9	0.09928(6)	0.7353(1)	0.72031(2)	0.0110(3)
Bi10	0.92832(6)	0.5681(1)	0.71886(2)	0.0122(3)
Bi11	0.93545(6)	0.2365(1)	0.71580(2)	0.0130(3)
Bi12	0.74800(6)	0.2240(1)	0.78030(2)	0.0126(3)
Bi13	0.77340(6)	0.3936(1)	0.71480(2)	0.0137(3)
Bi14	0.76527(7)	0.0626(1)	0.71854(2)	0.0129(3)
Bi15	0.38956(7)	0.0812(1)	0.08835(2)	0.0151(3)
Bi16	0.40269(6)	0.4138(1)	0.09647(2)	0.0107(3)
Bi17	0.37832(6)	0.7653(1)	0.09083(2)	0.0109(3)
Bi18	0.56112(6)	0.2247(1)	0.09581(2)	0.0129(3)
Bi19	0.55043(6)	0.9023(1)	0.10120(2)	0.0116(3)
Bi20	0.72829(6)	0.7589(1)	0.09322(2)	0.0120(3)
Bi21	0.72543(6)	0.4367(1)	0.08413(2)	0.0154(3)
Bi22	0.29976(6)	0.0792(1)	0.01978(2)	0.0111(3)
Bi23	0.29401(6)	0.7556(1)	0.03112(2)	0.0133(3)
Bi24	0.62639(6)	0.0425(1)	0.03960(2)	0.0136(3)
Bi25	0.621636)	0.7366(1)	0.03137(2)	0.0102(3)
Bi26	0.95130(6)	0.0734(1)	0.03002(2)	0.0105(3)
Bi27	0.95929(6)	0.4048(1)	0.02729(2)	0.0153(3)
Bi28	0.97529(6)	0.7244(1)	0.03640(2)	0.0116(3)
O1	0.819(1)	0.409(2)	0.1115(3)	0.013(4)
O2	0.0380(9)	0.613(1)	0.0623(3)	0.004(3)
O3	0.343(1)	0.899(2)	0.0131(3)	0.015(4)
O4	0.312(1)	0.871(1)	0.0643(3)	0.012(4)
O5	0.696(1)	0.402(2)	0.1427(3)	0.014(4)
O6	0.376(1)	0.107(1)	0.9928(3)	0.007(4)
O7	0.769(1)	0.601(1)	0.0745(3)	0.012(4)
O8	0.339(1)	0.269(2)	0.1057(4)	0.012(4)
O9	0.674(1)	0.364(2)	0.1949(3)	0.014(4)
O10	0.461(1)	0.274(1)	0.0799(3)	0.007(3)
O11	0.880(1)	0.576(1)	0.1440(3)	0.012(4)
O12	0.246(1)	0.603(2)	0.3256(3)	0.008(4)
O13	0.828(1)	0.207(1)	0.7070(2)	0.006(3)
O14	0.205(1)	0.711(1)	0.7287(3)	0.012(4)
O15	0.449(1)	0.887(2)	0.1801(4)	0.015(5)
O16	0.681(1)	0.087(2)	0.7913(3)	0.017(4)
O17	0.586(1)	0.885(1)	0.0523(3)	0.010(4)
O18	0.010(1)	0.223(2)	0.0201(4)	0.017(4)
O19	0.486(1)	0.882(1)	0.1339(3)	0.011(4)
O20	0.372(1)	0.724(2)	0.1453(3)	0.014(4)
O21	0.511(1)	0.083(2)	0.1137(3)	0.010(4)
O22	0.397(1)	0.094(2)	0.0469(3)	0.014(4)
O23	0.890(1)	0.401(2)	0.7050(3)	0.012(4)
O24	0.393(1)	0.707(2)	0.0482(3)	0.012(4)
O25	0.447(1)	0.905(2)	0.0802(3)	0.014(4)
O26	0.529(1)	0.082(2)	0.0151(4)	0.022(5)
O27	0.199(1)	0.077(2)	0.7404(3)	0.011(4)
O28	0.862(1)	0.103(2)	0.2915(3)	0.007(4)
O29	0.737(1)	0.621(2)	0.1249(3)	0.013(4)
O30	0.752(1)	0.214(2)	0.1750(4)	0.018(4)
O31	0.115(1)	0.500(1)	0.1508(1)	0.018(4)
O32	0.221(1)	0.407(2)	0.1724(4)	0.027(5)
O33	0.100(1)	0.323(2)	0.179(4)	0.028(5)
O34	0.151(1)	0.302(2)	0.1365(4)	0.024(5)
O35	0.052(1)	0.915(2)	0.1685(4)	0.015(5)
O36	0.936(1)	0.997(2)	0.1487(4)	0.019(5)
O37	0.941(1)	0.799(2)	0.1729(4)	0.024(5)
O38	0.986(1)	0.822(2)	0.1300(4)	0.020(5)
O39	0.519(1)	0.699(2)	0.1065(3)	0.014(4)
O40	0.615(1)	0.656(2)	0.0750(4)	0.019(4)
O41	0.589(1)	0.516(2)	0.1098(4)	0.019(5)
O42	0.499(1)	0.542(2)	0.0730(4)	0.022(5)
O43	0.776(1)	0.985(2)	0.1056(3)	0.019(4)
O44	0.656(1)	0.059(2)	0.0899(4)	0.021(5)
O45	0.727(1)	0.160(2)	0.1254(4)	0.024(5)
O46	0.761(2)	0.175(2)	0.0793(5)	0.045(7)
O47	0.769(1)	0.992(2)	0.0219(4)	0.022(5)
O48	0.861(1)	0.925(2)	0.0541(4)	0.027(5)
O49	0.740(1)	0.829(2)	0.0511(4)	0.028(5)
O50	0.821(1)	0.802(2)	0.0163(4)	0.024(5)
O51	0.130(1)	0.831(2)	0.0018(3)	0.019(4)
O52	0.192(1)	0.933(2)	0.0376(3)	0.011(4)
O53	0.073(1)	0.005(2)	0.0202(4)	0.017(5)
O54	0.088(1)	0.819(2)	0.0462(4)	0.020(5)
O55	0.130(2)	0.505(3)	0.2409(5)	0.05508)
O56	0.098(1)	0.719(2)	0.2417(5)	0.033(7)
O57	0.138(2)	0.633(2)	0.2019(5)	0.062(8)
O58	0.028(2)	0.582(3)	0.2123(8)	0.133(18)
O59	0.863(1)	0.083(2)	0.1971(5)	0.042(7)
O60	0.988(1)	0.141(2)	0.2074(5)	0.051(7)
O61	0.896(1)	0.200(2)	0.2367(5)	0.038(7)
O62	0.930(1)	0.983(2)	0.2335(4)	0.044(8)

$Bi_{14}P_4O_{31}$ represents the first member of the series proposed to explain the large domain of 'fluorite-type solid solution' observed in the Bi_2O_3–M_2O_5 (M = P, V) systems [13]. The building principle considers that the structures are built up by the stacking of two types of layers with the composition $[Bi_{18}O_{27}]$ and $[Bi_{14}M_4O_{31}]$ (M = P, V), respectively [13]. The general formula can be expressed as $Bi_{18-4m}M_{4m}O_{27+4m}$ with M = P, V and where the parameter m ($0 \leqslant m \leqslant 1$) represents the ratio of the number of $[Bi_{14}M_4O_{31}]$ layers to the total number of layers. One limit of the series ($m = 1$) corresponds to the composition $Bi_{14}M_4O_{31}$ where all the layers have the same composition as it is observed in the structure of $Bi_{14}P_4O_{31}$. The member $Bi_{46}M_8O_{89}$ corresponds to $m = 2/3$ where the sequence is 2 $[Bi_{14}M_4O_{31}]$ layers + 1 $[Bi_{18}O_{27}]$ layer [13]. In order to confirm and to demonstrate the efficiency of the structural model we carried out the synthesis of the member $Bi_{50}V_4O_{85}$ which should correspond to $m = 1/3$ and therefore to the sequence: 1 $[Bi_{14}V_4O_{31}]$ layer + 2 $[Bi_{18}O_{27}]$ layers.

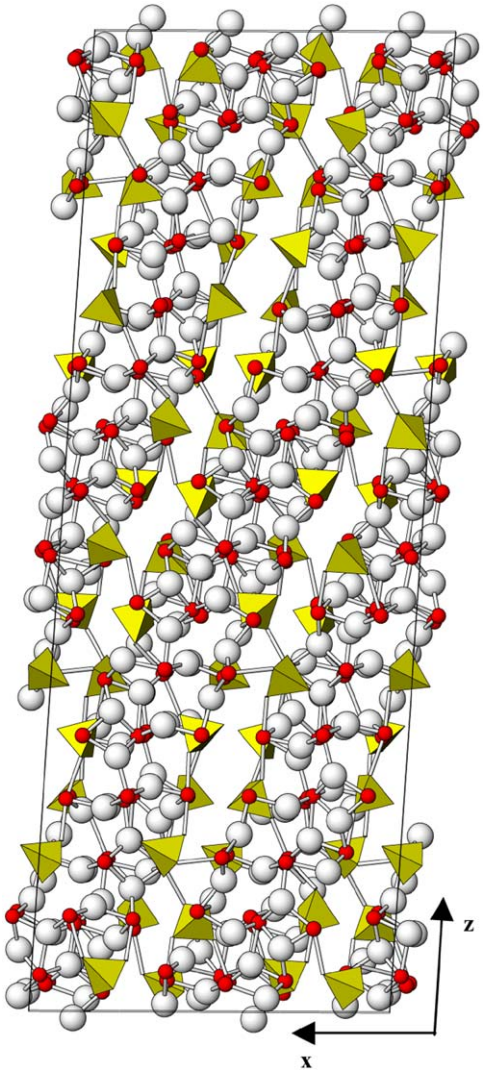

Fig. 2. Projection of the structure of $Bi_{14}P_4O_{31}$ on the (010) plane.

Table 3
Bond lengths (Å) for PO4 tetrahedra in $Bi_{14}P_4O_{31}$

P1–O31	1.47(2)	P1–O32	1.51(2)	P1–O33	1.61(2)
P1–O34	1.58(2)	P2–O35	1.57(2)	P2–O36	1.51(2)
P2–O37	1.59(2)	P2–O38	1.51(2)	P3–O39	1.56(2)
P3–O40	1.58(2)	P3–O41	1.50(2)	P3–O42	1.56(2)
P4–O43	1.50(2)	P4–O44	1.54(2)	P4–O45	1.55(2)
P4–O46	1.57(3)	P5–O47	1.46(2)	P5–O48	1.54(2)
P5–O49	1.57(2)	P5–O50	1.53(2)	P6–O51	1.54(2)
P6–O52	1.51(2)	P6–O53	1.54(2)	P6–O54	1.54(2)
P7–O55	1.55(3)	P7–O56	1.52(2)	P7–O57	1.51(3)
P7–O58	1.50(4)	P8–O59	1.51(2)	P8–O60	1.51(2)
P8–O61	1.58(3)	P8–O62	1.59(2)		

3.2. $Bi_{50}V_4O_{85}$

The X-ray powder diffraction pattern of $Bi_{50}V_4O_{85}$ obtained after quenching at 920 °C is given in Fig. 5a. All the main peaks are characteristic of a pseudo-cubic fluorite type structure with $a_c \approx 5.5$ Å. However a careful examination of the XRD at low θ-values clearly shows weak peaks that cannot be indexed in the pseudo

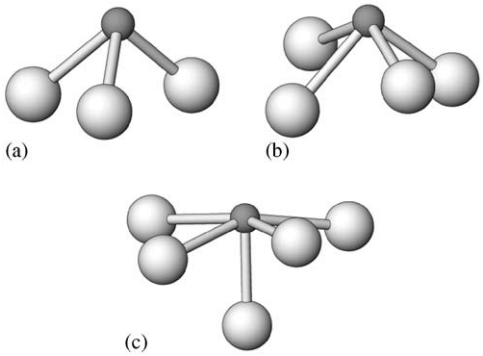

Fig. 3. Polyhedra around the bismuth in $Bi_{14}P_4O_{31}$ (a) CN = 3, (b) CN = 4, and (c) CN = 5.

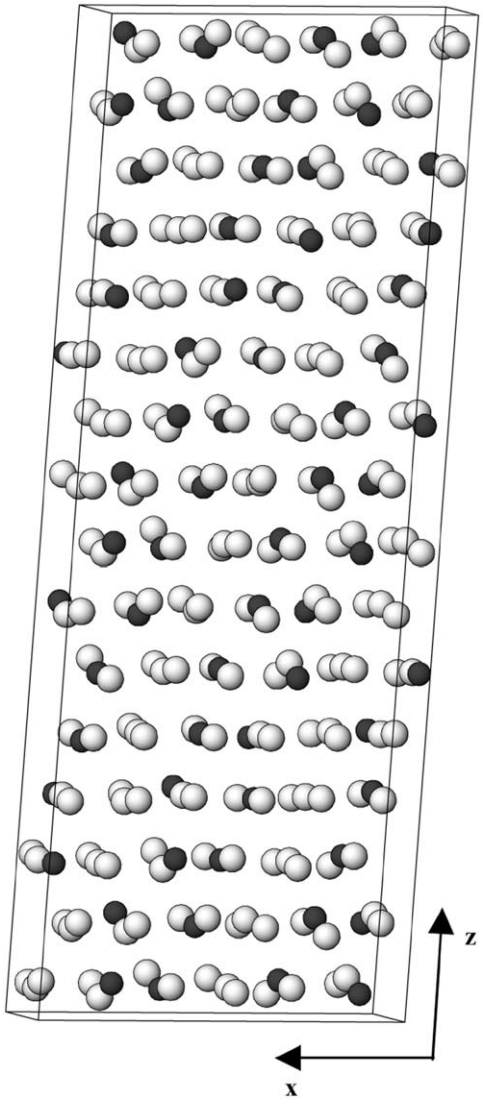

Fig. 4. Stacking of the $[Bi_{14}P_4O_{31}]$ layers along the *c*-axis. The oxygen atoms have been omitted for clarity.

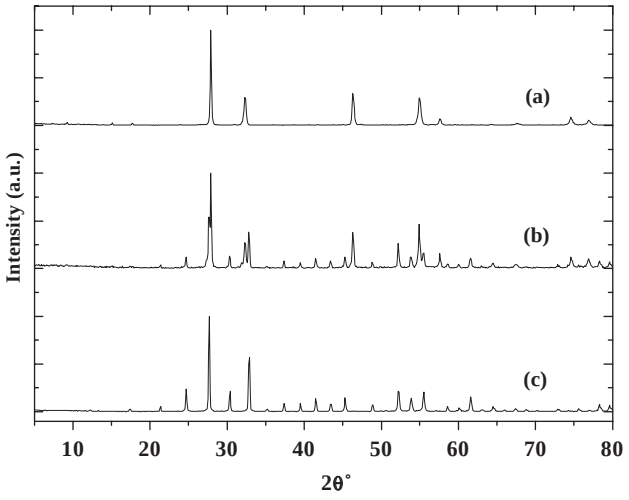

Fig. 5. (a) XRD pattern of $Bi_{50}V_4O_{85}$ after quenching at 920 °C; (b) after quenching at 800 °C; and (c) XRD pattern of a sillenite phase for $r = Bi/P = 14$.

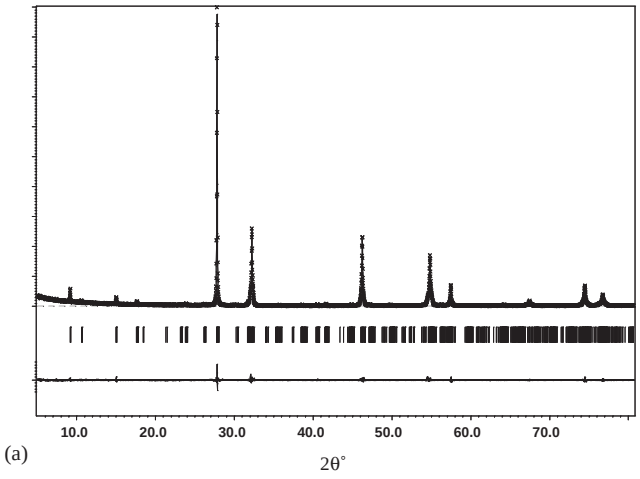

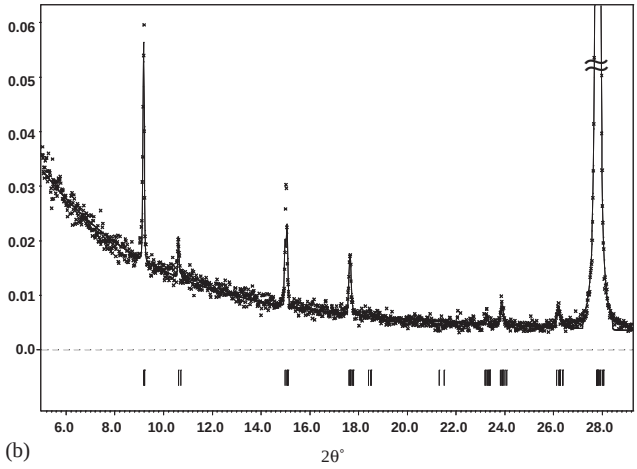

Fig. 6. (a) Profile matching for $Bi_{50}V_4O_{85}$; and (b) zoom at low 2θ-angles.

cubic fluorite. It has been shown that $Bi_{50}V_4O_{85}$ is only stable at high temperature. Indeed, the XRD pattern after an annealing at 800 °C (48 h) is totally different and corresponds to a mixture of two phases (Fig. 5b). One corresponds to a cubic sillenite phase (Fig. 5c) and the second one to a pseudo-cubic fluorite. The transformation is reversible and achieved with a change of colour from yellowish for $Bi_{50}V_4O_{85}$ to orange colour for the low temperature mixture. Therefore, the preparation of single crystals seems to be problematic. However, crystals have been grown by melting the phase at 970 °C followed by a slow cooling (5 °C/h) down to 800 °C and then cooled rapidly to room temperature.

Many crystals have been tested on the Enraf-Nonius Kappa CCD diffractometer and systematically, the standard peak search shows a *I*-centred monoclinic symmetry with lattice parameters $a = 11.8144(2)$ Å, $b = 11.7548(2)$ Å, $c = 16.5043(2)$ Å, and $\beta = 90.27(1)^\circ$. The XRD powder pattern of $Bi_{50}V_4O_{85}$ has fully been indexed (Fig. 6a) as well as the very weak peak at low angles as shows the profile matching in Fig. 6b. These peaks are characteristic of the atomic ordering of Bi and V atoms in the monoclinic super-cell.

The *I* centred monoclinic cell (a, b, c) can be transformed in a standard *C*-centred monoclinic cell (a', b', c') using the well known following vector equations: $\mathbf{a}' = \mathbf{a} + \mathbf{c}$, $\mathbf{b}' = \mathbf{b}$ and $\mathbf{c}' = -\mathbf{a}$. The new lattice parameters are: $a' = 20.2518$ Å, $b' = 11.7548$ Å, $c' = 11.8144$ Å and $\beta = 125.42^\circ$. They are related to the cubic unit cell of the fluorite (a_c) by the vector relations: $\mathbf{a}' = 1.5\mathbf{a}_c + 1.5\mathbf{b}_c + 3\mathbf{c}_c$, $\mathbf{b}' = 1.5\mathbf{a}_c - 1.5\mathbf{b}_c$ and $\mathbf{c}' = 0.5\mathbf{a}_c + 0.5\mathbf{b}_c - 2\mathbf{c}_c$. The value of the determinant of the transformation, 13.5, implies that the volume of the monoclinic cell is 13.5 times the volume of the pseudo-*fcc* subcell. Since the *fcc* fluorite cell contains four cations, there are $4 \times 13.5 = 54$ cations in the monoclinic cell. This result is in good agreement with the formula $Bi_{50}V_4O_{85}$ with $Z = 1$. The second observation that can be done concerns the value of the c parameter more precisely the value of $c \sin\beta$. This value, to agree with the model, must be equal to a constant corresponding to the interlayer distance times an integer. For example, the lattice parameters of $Bi_{46}V_8O_{89}$ are: $a = 20.0100(4)$ Å, $b = 11.6445(4)$ Å, $c = 20.4136(4)$ Å and $\beta = 107.27(3)^\circ$ and the structure corresponds to the stacking along the c-axis of six atomic layers [13]. It results in a calculated interlayer distances of 3.25 Å ($c \sin\beta = 19.49$ Å $= 6 \times 3.25$ Å). The value of 3.23 ± 2 Å can be considered as the reference. For $Bi_{50}V_4O_{85}$ the value of $c' \sin\beta$ is equal to 9.63 Å which leads to a stacking sequence along the c'-axis of three atomic layers (9.63 Å $= 3 \times 3.21$ Å). The unique way to combine the number of cations in the unit cell (54 cations) and the number of atomic layers in the sequence is to consider the following distribution of 2 $[Bi_{18}O_{27}]$

layers + 1 [$Bi_{14}V_4O_{31}$] layer. An other conclusion that can be done concerns the number of oxygen atoms in the elementary structure which is odd in this case and as the Bravais lattice is *C* (or *I*) centred, at least one oxygen atomic position in the structure is partially occupied. Consequently, one can expect oxide-ion conduction for $Bi_{50}V_4O_{85}$ as it will be shown in the next paragraph.

An attempt to solve accurately the structure of $Bi_{50}V_4O_{85}$ on single crystal has been carried out. Unfortunately, the quality of the crystals is not so good to get an accurate determination of the structure, especially on the oxygen positions. An explanation could be the method of preparation of the crystals which is imposed by the thermal stability of $Bi_{50}V_4O_{85}$. Other methods of preparation of single crystals as flux method, for example, are in progress in order to improve the quality of the crystals. However, from the single crystal selected, it has been possible to determine the repartition of the heavy atoms. The Bi and V atoms are well ordered and as expected, constitutes three atomic layers along the *c*-axis (Fig. 7). The oxygen positions were deduced from Fourier map. The refinement converges to a *R*-value of $R = 0.089$ for 2291 independent reflections considering only anisotropic displacement parameters (ADP) for the Bi and V atoms. All the atomic ADP are defined but systematic too high ($U_{iso} \approx 0.1$ Å^2) which is the signature of strong atomic constraints in the crystal. Especially for the VO_4 tetrahedron, three oxygen atoms have systematically been split in two positions to interpret the electronic density around the vanadium atoms. The two configurations of the VO_4 terahedron are related to each other by a rotation around a V–O bond. Although the structure is highly disordered concerning the oxygen atoms, it is beyond doubt that the sequence corresponds to $m = 1/3$ and as expected the stacking is: 1 [$Bi_{14}V_4O_{31}$] layer + 2 [$Bi_{18}O_{27}$].

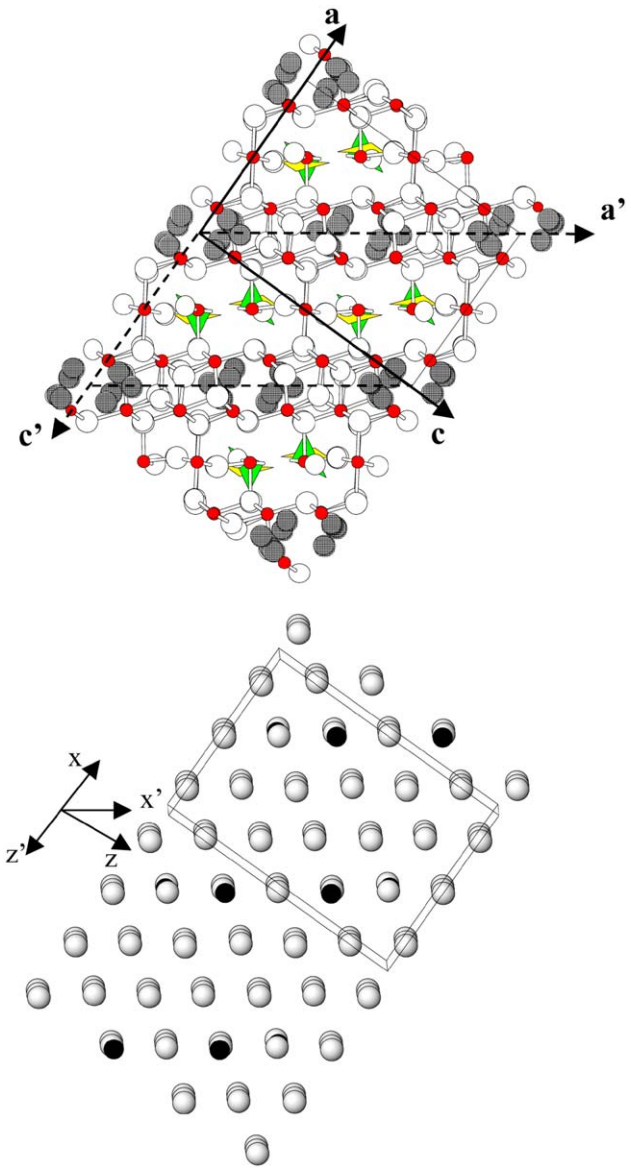

Fig. 7. (a) Projection of the $Bi_{50}V_4O_{85}$ on the (010) plane, black small circles (Bi), empty circles (○), black dashed circles (partially oxygen positions); (b) sequence of the [$Bi_{14}V_4O_{31}$] and [$Bi_{18}O_{27}$] layers along the *z*′-axis (*C*-centred unit-cell) or *x*-axis (*I*-centred unit-cell).

3.3. Ionic conductivity of $Bi_{14}P_4O_{31}$ and $Bi_{50}V_4O_{85}$

The previous conductivity measurements in the systems Bi_2O_3–M_2O_5 have been performed on the compounds, $Bi_{23}M_4O_{44.5}$ (M = P and V) by Watanabe in 1997 [8]. These bismuth oxides show a good oxide-ion conduction. In particular, $Bi_{23}V_4O_{44.5}$ is a good ionic conductor: $\sigma_{600} \approx 10^{-2}\,\Omega^{-1}\,cm^{-1}$, and shows a ionic transport number $t_i \approx 0.9$ at about 600 °C.

Typical impedance spectra of $Bi_{14}P_4O_{31}$ and $Bi_{50}V_4O_{85}$ samples are reported in Figs. 8 and 9, respectively. Concerning the phosphorous compound, the Nyquist plots show only one loop in all the temperature range. Referring to the associated capacitive effect (3×10^{-11} Farads), we can conclude that the chord of the observed high frequency semicircle can be related to the bulk contribution.

In the case of the vanadate $Bi_{50}V_4O_{85}$, two temperature ranges can be distinguished. For low temperatures, the Nyquist plots are characterised by a slightly depressed semi-circle, for the high frequency contribution, associated to straight lines at lower frequencies (Fig. 10). The high frequency part represents the bulk contribution of the $Bi_{50}V_4O_{85}$ ceramic and the straight line can be associated with interfacial processes at the gold electrodes. The bulk contribution was fitted to a simple parallel combination of a resistance *R* and a capacitance *C*. The mean value of calculated bulk capacitance is of about 2×10^{-11} Farads, in good agreement with that usually found for bulk response [19]. That is the reason why we assume that the resistance *R* of the high frequencies semi-circles represents the intra-granular response of the ceramic. Then,

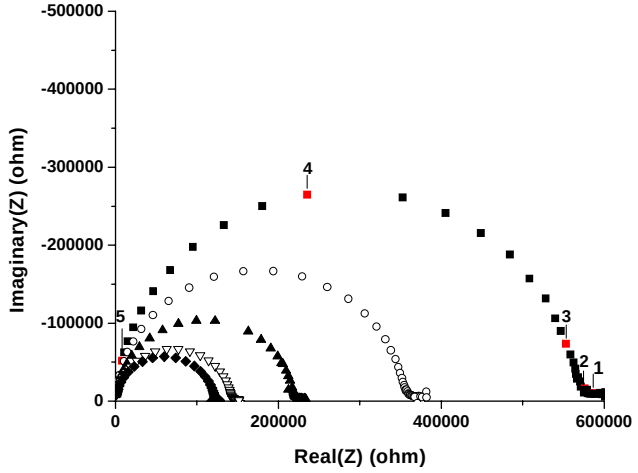

Fig. 8. Typical impedance diagrams obtained under air using symmetric cells with $Bi_{14}P_4O_{31}$ ceramic: (■) 403 °C, (○) 427 °C, (▲) 452 °C, (▽) 477 °C and (♦) 503 °C. The numbers indicate the measured frequency logarithm.

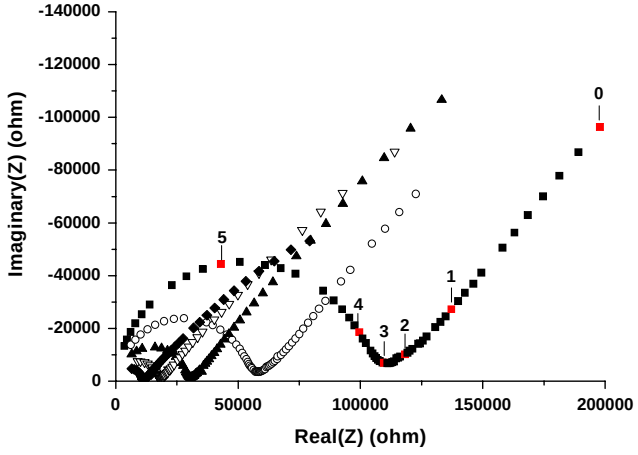

Fig. 9. Typical impedance diagrams obtained under air using symmetric cells with $Bi_{50}V_4O_{85}$ ceramic: (■) 403 °C, (O) 427 °C, (▲) 452 °C, (▽) 477 °C and (♦) 503 °C. The numbers indicate the measured frequency logarithm.

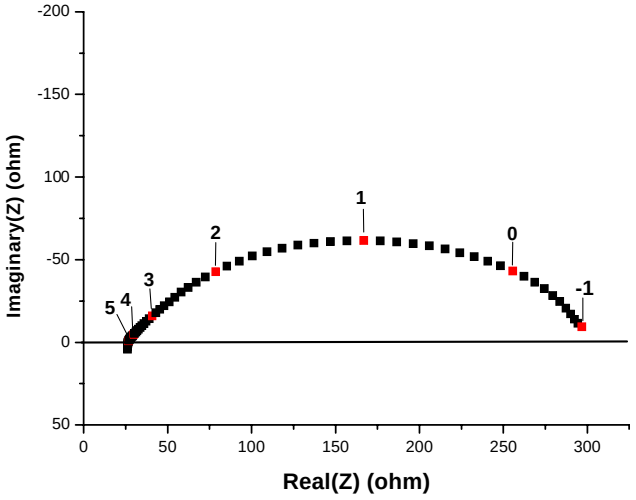

Fig. 10. Impedance diagrams obtained under air using symmetric cells for $Bi_{50}V_4O_{85}$ ceramic at 800 °C. The numbers indicate the measured frequency logarithm.

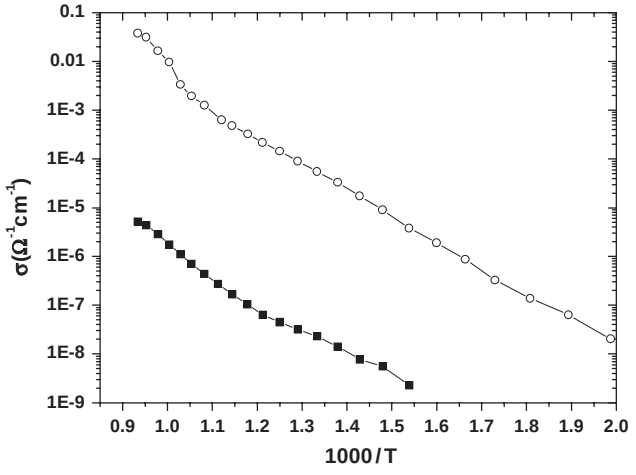

Fig. 11. Arrhenius plots of electrical conductivity of $Bi_{50}V_4O_{85}$ (○) and $Bi_{14}P_4O_{31}$ (■).

the bulk conductivity is calculated from the bulk resistance R according to the relation $\sigma = 1/R \times (L/S)$.

In the case of higher temperatures, the electrodes impedance becomes more important than bulk contribution (Fig. 11). The high frequency part intercept the bulk impedance associated to the inductive contribution of the platinum wires used as current collectors. Low frequencies contributions can be associated to the electrodes processes (Fig. 10).

The Arrhenius plot of the conductivity is shown in Fig. 11. The calculated conductivity values are $\sigma_{650} = 0.001\,\Omega^{-1}\,cm^{-1}$ for $Bi_{50}V_4O_{85}$, and $\sigma_{650} = 4 \times 10^{-7}\,\Omega^{-1}\,cm^{-1}$ for $Bi_{14}P_4O_{31}$. These results fully confirm the structural analysis and as expected $Bi_{50}V_4O_{85}$ is a good ionic conductor comparable to $Bi_{46}V_8O_{89}$. The activation energies observed for both compounds are nearly the same: $E_A = 1.05\,eV$ for $Bi_{50}V_4O_{85}$ compound and $E_A = 1.09\,eV$ for $Bi_{14}P_4O_{31}$. These values are closed to the activation energy measured on yttrium stabilised zirconia (YSZ) ($E_A \approx 1.00\,eV$) but higher than the value observed by Watanabe on $Bi_{23}V_4O_{44.5}$ ($E_A \approx 0.78\,eV$) [8].

4. Conclusions

An idealized structural model is proposed for materials related to the fluorite-type structure in the Bi_2O_3–M_2O_5 systems (M = P, V). The general formula is expressed $Bi_{18-4m}M_{4m}O_{27+4m}$ where the variable m

Table 4
Lattice parameters of compounds belonging to the series $Bi_{18-4m}M_{4m}O_{27+4m}$

Compound	a (Å)	b (Å)	c (Å)	β (°)	$c\sin\beta$ (Å) $= n.\Delta l$ (Å)
$Bi_{46}P_8O_{89}$ [13]	19.6073	11.4181	21.1119	112.14	$19.56 = 6 \times 3.26$
$Bi_{14}P_4O_{31}$ (this work)	19.2745	11.3698	52.4082	93.63	$52.30 = 16 \times 3.27$
$Bi_{46}V_8O_{89}$ [13]	20.0100	11.6445	20.4136	107.27	$19.49 = 6 \times 3.25$
$Bi_{50}V_4O_{85}$ (this work)	20.2518	11.7548	11.8144	125.42	$9.63 = 3 \times 3.21$
"$Bi_{14}V_4O_{31}$" [20]	19.7200	11.4590	80.1600	90.50	$80.16 = 25 \times 3.21$

Relationships between the $c\sin\beta$ value and the interlayer distance.

($0 \leqslant m \leqslant 1$) defines the ratio of the number of $[Bi_{14}M_4O_{31}]$ over the total number of layers in the sequence. It has been shown that the structures of the two new compounds $Bi_{14}P_4O_{31}$, $Bi_{50}V_4O_{85}$ and $Bi_{46}M_8O_{89}$ ($M = P$, V) belong to this family and correspond to the members $m = 1, 1/3$ and $2/3$, respectively. All the structures have a monoclinic symmetry and are characterized by a cationic ordering of the bismuth and the M atoms ($M = P$, V) in the framework. The M atoms occupy tetrahedra which are well isolated to ones from the others. The building principle lays down that the a and b lattice parameters must be almost constant whatever the m value (Table 4). They are related to the cubic parameter of the fluorite-type by the metric relation: $a \approx 3\sqrt{6}/2a_c \approx 20\,\text{Å}$ and $b = 3\sqrt{2}/2a_c \approx 11.7\,\text{Å}$. The variable parameter is $c\sin\beta$ which defines the periodicity of the atomic layers stacking. The value of $c\sin\beta$ must be an integer times the interlayer distance which has been averaged to $\approx 3.23\,\text{Å}$ (Table 4). This last condition on the $c\sin\beta$ value is perfectly confirmed by the material identified as '$Bi_{14}V_4O_{31}$' [20]. The symmetry is also monoclinic but no structural details were given. If we are perplex on the composition of the phase, one notices that the lattice parameters fit very well the conditions (Table 4). The stacking along the c-axis corresponds to 25 atomic layers. It is predictable and well known from other structural systems based also on periodic layer stackings that when the period becomes too long stacking faults can be evidenced at the microstructural scale and even modulated phases can be observed as it has been observed in the Bi_2O_3–V_2O_5 system [5]. One can expect to be possible to imagine a unique model using the superspace formalism where both commensurate or incommensurate structures are idealized as it has been done, for example, for the related 2H hexagonal perovskite [21]. However, before to establish such a model, more experimental results are absolutely necessary to clarify the contradictory results published on these systems [1–9]. Works are in progress in this way.

5. Supporting information available

Further details of the crystal structure investigation can be obtained from the supporting information available from the Fachinformationszntrum Karlsruhe, 76344 Eggenstein-Leopoldshafen, Germany, (fax: (49) 7247-808-666; email: mailto:crysdata@fiz-karlsruhe.de) on quoting the depository number CSD-415115.

References

[1] L.H. Brixner, C.M. Foris, Mater. Res. Bull. 8 (1973) 1311.
[2] L.W. Zhou, D.A. Jefferson, J.M. Thomas, Proc. R. Soc. London, Ser. A 406 (1986) 173.
[3] W. Zhou, D.A. Jefferson, J.M. Thomas, J. Solid State Chem. 70 (1987) 129.
[4] W. Zhou, J. Solid State Chem. 76 (1988) 290.
[5] W. Zhou, J. Solid State Chem. 87 (1990) 44.
[6] S. Kashida, T. Hori, K. Nakamura, J. Phys. Soc. Japan 63 (1994) 4422.
[7] S. Kashida, T. Hori, J. Solid State Chem. 122 (1996) 358.
[8] A. Watanabe, Solid State Ionics 96 (1997) 75.
[9] A. Watanabe, Y. Kitami, Solid State Ionics 113–115 (1998) 601.
[10] T.E. Crumpton, M.G. Francesconi, C. Greaves, J. Solid State Chem. 175 (2003) 197.
[11] H.A. Harwig, Z. Anorg. Allg. Chem. 444 (1978) 151.
[12] G. Gattow, H.Z. Schröder, Z. Anorg. Allg. Chem. 318 (1962) 176.
[13] J. Darriet, J.C. Launay, F.J. Zúñiga, J. Solid State Chem. in press.
[14] J.L. Soubeyroux, M. Devalette, N. Khachani, P. Hagenmuller, J. Solid State Chem. 86 (1990) 59.
[15] S.F. Radaev, V.I. Simonov, Yu.F. Kargin, Acta Crystallogr. B 48 (1992) 604.
[16] A. Le Bail, H. Duroy, J.L. Fourquet, Mater. Res. Bull. 23 (1988) 447.
[17] V. Petricek, M. Dusek, The Crystallographic Computing System Jana 2000, Institute of Physics, Praha, Czech Republic.
[18] P. Thompson, D.E. Cox, J.B. Hastings, J. Appl. Crystallogr. 20 (1987) 79.
[19] J.R. Mac Donald, Impedance Spectroscopy Emphasizing Solid Materials and Systems Ed., Wiley, New York, 1987.
[20] T.V. Panchenko, V.F. Katkov, V. Kh. Kostyuk, N.A. Truseeva, A.V. Schmal'ko, Ukr. Fiz. Zh. (Russ. Ed.) 28 (7) (1983) 1091.
[21] J.M. Perez-Mato, M. Zakhour-Nakhl, F. Weill, J. Darriet, J. Mater. Chem. 9 (1999) 2795.